

Tight-Binding realization of non-abelian gauge fields: singular spectra and wave confinement

Y. Hernández-Espinosa

Universidad Nacional Autónoma de México, Instituto de Física, Apartado Postal, 04510 Ciudad de México

E. Sadurní

Benemérita Universidad Autónoma de Puebla, Instituto de Física, Apartado Postal J-48, 72570 Puebla, México

(Dated: June 11, 2021)

We present a geometric construction of a lattice that emulates the action of a gauge field on a fermion. The construction consists of a square lattice made of polymeric sites, where all clustered atoms are identical and represented by potential wells or resonators supporting one bound state. The emulation covers both abelian and non-abelian gauge fields. In the former case, Hofstadter's butterfly is reproduced by means of a chain made of rotating dimers, subject to periodic boundary conditions parallel to the chain. A rigorous map between this model and Harper's Hamiltonian is derived. In the non-abelian case, band mixing and wave confinement are obtained by interband coupling using $SU(2)$ as an internal group, *i.e.* the effects are due to non-commutability of field components. A colored model with $SU(3)$ made of trimers is also studied, finding thereby the appearance of flat bands in special configurations. This work constitutes the first all-geometric emulation of the Peierls substitution, and is valid for many types of waves.

CONTENTS

I. Introduction	1
II. Presentation of results	2
III. Internal degrees of freedom: gauge group obtained from the lattice	4
A. General theory on the lattice	4
B. Decomposition in terms of external lattice couplings and internal polymeric couplings	7
IV. Emulation of Peierls substitution for $U(1)$ gauge field	7
A. Linear chain	7
V. Emulation of $SU(2)$ field	11
A. A model with $SU(2)$	11
B. Effective negative couplings and level inversion revisited	12
C. Wave confinement in $SU(2)$. Bound states	13
VI. Band mixing in $SU(3)$ models with color	13
VII. Conclusion	14
Acknowledgments	15
A. Unitary map between translation operators in 1D; beyond Aubry's duality.	15
B. Box-counting fractal dimension calculation	16
References	16

I. INTRODUCTION

The realization of Yang-Mills theories in lattices is the ultimate goal of spectral quantum emulations [1]. The standard model of particles and fields rests on the assumption that internal degrees of freedom such as color are dynamically responsible for the emergence of composite structures in the form of baryons and mesons [2]. Lattice QCD is indeed a dynamical description of such theories, where the numerical work is meant to show the emergence of color confinement [3] and infrared slavery [4–6]. However, the implementation of gauge symmetry on the lattice must be done with a proper generalization of Peierls' substitution that incorporates internal degrees of freedom such as color or isospin. In this paper we take care of this aspect, as the lattice emulations presented are sufficiently simple to illuminate important aspects of gauge fields that can be implemented by purely geometrical manipulations of sites on the crystal.

Previous steps towards this goal are the use of atomic levels in experiments involving atomic fountains and the interaction of atoms with the radiation field [7, 8]. We also find optical realizations of abelian gauge fields –e.g. the typical electromagnetic field– where photons in coupled waveguides [9] play the role of a Schrödinger wave under the action of an external force. Complex hopping amplitudes have also been obtained by means of laser techniques [10], and internal degrees of freedom in coupled waveguides have been used with similar purposes [11]. However, as far as we can see, there has been no attempt to produce these models on a homogeneous lattice without any other assumption than a single quantum state per site. We also take this opportunity to look at microwave realizations with dielectric resonators supporting a single trapped mode. These have been experimentally successful in the emulation of solid state systems such as graphene and boron nitride, which con-

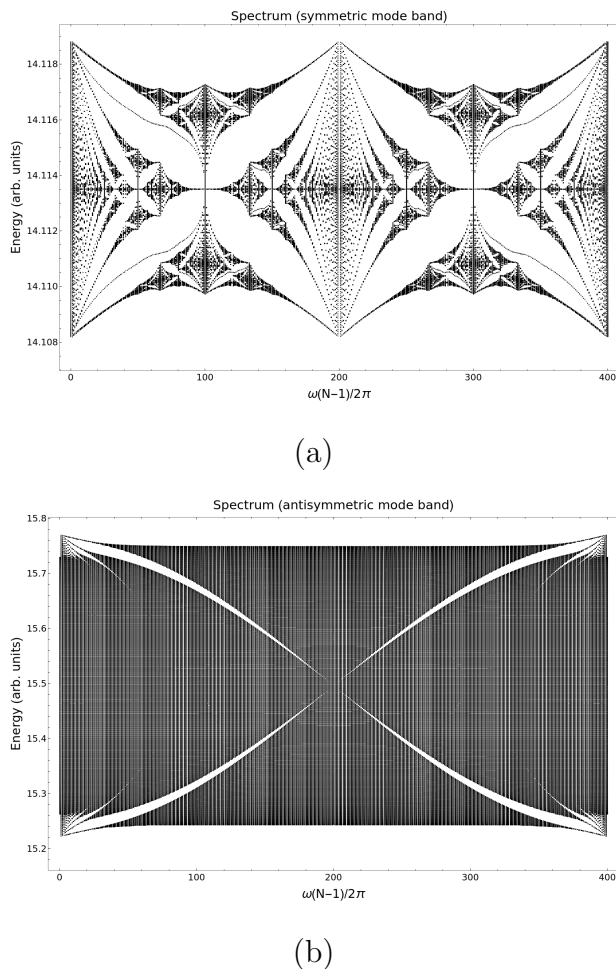


FIG. 1. (a) The spectrum of the decoupled symmetric band for a chain of 801 dimers. The Hofstadter butterfly emerges in the first quarter of the frequency range $\omega(N-1)/2\pi$. The geometric values are $L = 1.66$, $d = 0.1$ and $\lambda = 1.66$ (b). The spectrum of the decoupled antisymmetric band where the Harper's Hamiltonian is emulated for $\Lambda = 0.08 \cos \omega$. The geometric values are $L = 2.8$, $d = 0.35$ and $\lambda = 1$. Energy is in arbitrary units.

stitute yet another mesoscopic testbed for relativistic spectral emulations [12–19] using the celebrated analogy between the Dirac equation and structures with Dirac points [20–24].

Our task now is to emulate gauge fields using real scalar waves, starting with the abelian case. We shall see, on the fly, that the procedure giving rise to complex couplings can be employed to produce non-abelian theories as well. With this, we take a step further in our quest for universal emulations using a single-level atom and purely geometrical manipulations.

We focus on the fermionic part of a non-abelian Yang-Mills theory, where the bosonic part is treated as a static field. The Yang-Mills Lagrangian for vector fields inter-

acting with fermions is:

$$\mathcal{L} = \bar{\psi} i \gamma^\mu \partial_\mu \psi - m \bar{\psi} \psi + \bar{\psi} \gamma^\mu g A_\mu^a \tau_a \psi - \frac{1}{4} (F_{\mu\nu}^a)^2 \quad (1)$$

$$F_{\mu\nu} = \partial_\mu A_\nu - \partial_\nu A_\mu - ig [A_\mu, A_\nu], \quad F_{\mu\nu} = F_{\mu\nu}^a \tau_a. \quad (2)$$

As is well-known, the Dirac lagrangian $\bar{\psi} i \gamma^\mu \partial_\mu \psi - m \bar{\psi} \psi$ has been emulated in 2+1 dimensions using hexagonal lattices of one species (graphene, massless case) and two species (boron nitride, massive case). For simplicity we pursue an emulation of non-abelian fields acting on a fermion hopping on a square lattice. Therefore, our attention is focused on the first and second terms of (1), but this time formulated as a Peierls non-abelian gauge field. The internal degrees of freedom due to the gauge group will be introduced by means of polymeric sites, i.e. clusters of single-level atoms regarded as a single cell in a crystal. In this respect, the term $(F_{\mu\nu}^a)^2$ will be assumed to be fixed and static.

Structure of the paper: section II presents the main results of our emulations for fields U(1), SU(2) and SU(3) with different tight-binding systems made of dimers and trimers. In section III we discuss the construction of lattices with internal degrees of freedom using the energy levels of polymeric structures. Section IV is dedicated to the emulation of the U(1) abelian field using linear chains of rotating dimers. The emulation of the non-abelian field SU(2) is presented in section V, where the phenomenon of wave confinement in a square lattice of dimers is achieved. The non-abelian vector field \mathbf{A} and the component B_z of the field are plotted. Section VI contains some numerical results of the spectrum obtained from linear chains of rotating trimers.

II. PRESENTATION OF RESULTS

In quantum field theory the magnetic field is considered the starting point in the study of gauge invariance. Our first step is the emulation of the abelian U(1) theory.

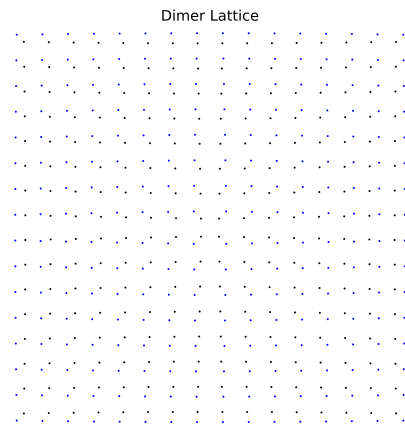


FIG. 2. Hedgehog type lattice.

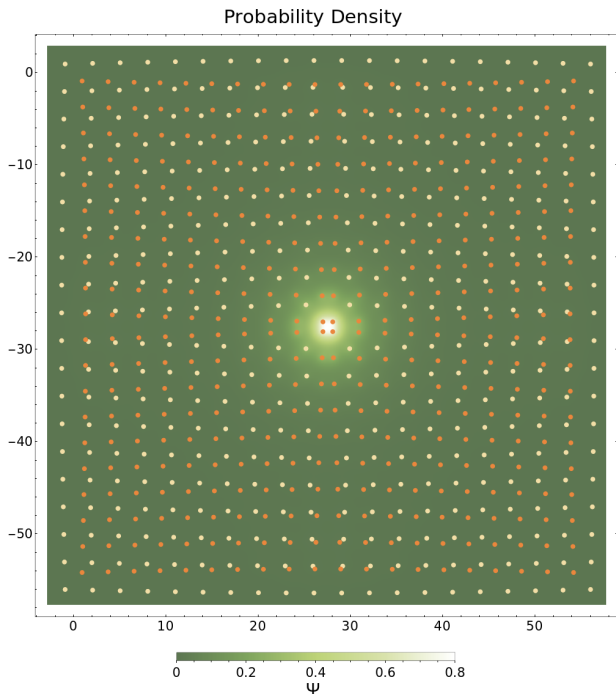


FIG. 3. Square lattice with localized wave function at the center. The dimers are presented as a guide to the eye. The highest energy state displays the localization effect. The dimers are made of orange (dark) and yellow (light) dots, presented as a guide to the eye. The parameters are $L = 2.9$, $d = 1.3$ and $\lambda = 1$.

Historically, the effects of an external magnetic field acting on a two-dimensional lattice were studied by Peierls [25] and later by Harper [26]. The Harper model is a particular case of the Almost Mathieu Operator (AMO) [27], where the irrationality of the magnetic flux per unit cell plays an important role in the shape of the spectral set. In 1964 [28] Azbel found that in a lattice with an external magnetic field, each Landau level in the spectrum of the particle splits successively into sublevels. In 1976 Hofstadter found strong evidence of the fractal nature of the spectrum and subsequently it was proved that the spectral set must be a Cantor dust with zero Lebesgue measure [29]. Emulations of the so-called Hofstadter butterfly have been proposed in acoustic systems [30, 31] and microwave scatterers [32].

U(1) EMULATION WITH DIMER CHAINS. We proceed with a construction of linear chains made of rotating dimers within a nearest-neighbor tight-binding description. In this artificial realization, the number of complete turns p of one dimer along the chain is the analog of the ω frequency –or magnetic flux– in Harper’s Hamiltonian. These chains exhibit singular spectra for specific lattice parameters, such as the distance between centers of neighboring dimers and the length of each dimer. Due to the internal degrees of freedom of each array site, the spectrum shows coupled bands. Two cases can be distinguished here: *i*) if the bands are strongly coupled, the

non-abelian nature of the field emerges and *ii*) when these two bands are completely decoupled, we recover independent U(1) theories. The latter case is illustrated in Fig. 1. The electronic structure can be studied properly if we write the Hamiltonian H in the basis of symmetric and antisymmetric states of each dimer, and reorganize it into a block-diagonal form of couplings between symmetric levels (S–S) and antisymmetric levels (A–A). The spectrum generated by the S–S block is presented in panel (a) of Fig. 1, where the Hofstadter butterfly appears. This case emulates a magnetic field piercing through a square lattice and corresponds to $\Lambda = 1$ in the AMO. On the other hand, panel (b) shows the spectrum of a magnetic field in a rectangular lattice, in this case Λ is approximately $0.08\cos\omega$. Both spectra show invariance when periodic boundary conditions are imposed, which is in agreement with the independence of the spectrum on Bloch’s quasi-momentum k along the periodic direction of a square lattice under the effect of an external magnetic field in the Landau gauge. It has been proved that the spectrum of the AMO is a Cantor set [33], so in order to complete the analogy of our system with the Harper’s model, we report the fractal dimensions of the antisymmetric and symmetric bands for fixed values of $\omega(N - 1)/2\pi$ in Fig. 14 and Table I respectively.

SU(2) EMULATION AND WAVE CONFINEMENT. The hypothesis of color confinement in quantum chromodynamics (QCD) establishes that only color-neutral multiplets of SU(3) can be observed. In the same spirit of the previous section, we construct a square lattice made of dimers in order to emulate the phenomenon of localization in SU(2). Although wave localization has been studied also in disordered arrays –Anderson localization– we are interested here in stronger effects, e.g. bound states localized around a central point. The lattice is illustrated in Fig. 2 and the details of its construction will be discussed in section V. Figure 3 shows the localized wave function of

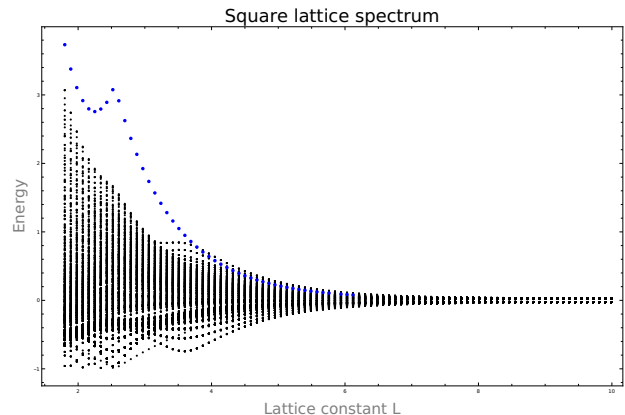


FIG. 4. Spectrum of the hedgehog type lattice as a function of lattice parameter L . Blue points represent localized states at the center of the array as shown in Fig. 3. This state merges with one of the bands as the interdimer distance increases.

the highest energy state on a lattice made of 400 dimers, whose sites are included as spatial reference. We can observe that the confinement manifests around the region with the strongest couplings. This localized state coalesces with the propagation band and disappears in the limit when the lattice constant –distance between dimer centers– is much greater than the length of the dimer *i.e.* the fully periodic case without any internal structure.

LINEAR CHAIN WITH SU(3). Analogously to the linear chain of dimers, the SU(3) case can be studied by adding more degrees of freedom to each site. We propose a polymer of nine sites illustrated in Fig. 13. Some interesting results arise from this model. The spectrum of the system consists of three bands and two of them are overlapped as shown in Fig. 5 panels a) and b). The upper band shows fractal structure consistent with Hofstadter’s butterfly, while the lower band shows a dense structure with no recognizable pattern. The unitary cell of the chain consists of a trimer made of trimers as shown in Fig. 13. The separation of the bands can be performed by symmetry breaking of *i)* the global C_3 symmetry by rotation of only one internal trimer and *ii)* internal C_3 symmetry by deformation of the internal trimers. In panel c) of Fig. 5 the lower part of the spectrum shows four decoupled bands with very small bandwidths. The study of superconductivity associated with flat bands might be of interest, as shown elsewhere[34]. In our case, the spectrum shows localized states around specific energy values when the magnetic flux varies.

III. INTERNAL DEGREES OF FREEDOM: GAUGE GROUP OBTAINED FROM THE LATTICE

The results presented in section II provide evidence of a U(1) field emulation on two-dimensional lattices and the localization phenomenon in the SU(2) case. In order to properly formulate gauge fields in tight-binding arrays, the analog of minimal coupling in discrete systems must be introduced. This section is devoted to such formalism in discrete space with their correct laws of transformation, including non-abelian fields.

A. General theory on the lattice

The usual treatment in continuous variables includes non-abelian fields $A_\mu = A_\mu^\sigma \tau_\sigma$, with μ a space-time index, σ a group index and τ the generators of SU(N). The minimal coupling prescription for space and time, ensures the gauge invariance of a theory involving charged particles and dynamical bosonic fields

$$p_\mu \mapsto p_\mu + gA_\mu, \quad \mathbf{p} \mapsto \mathbf{p} + g\mathbf{A}. \quad (3)$$

This can be specialized to static fields where the 0-th component is irrelevant (purely magnetic); this is ex-

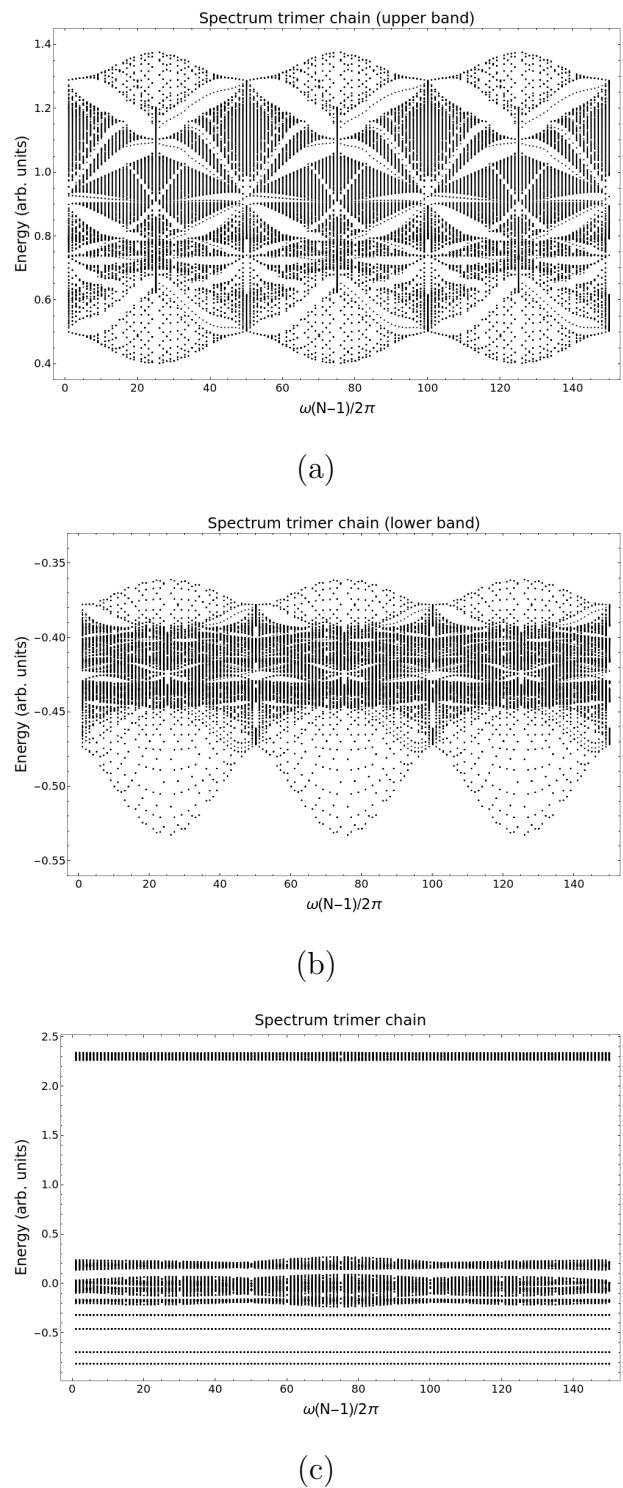


FIG. 5. The spectra of a linear chain made of trimers. The unit cell of the chain is illustrated in Fig. 13. a) The upper part of the spectrum is made of two overlapped bands. A fractal structure can be distinguished, resembling a Hofstadter’s butterfly. b) Lower part of the spectrum. The band is dense and shows no recognizable structure. c) Spectrum with internal and global C_3 broken symmetry. The lower bands are flat.

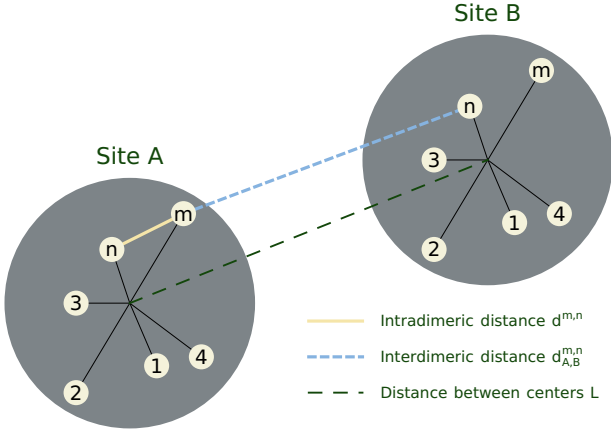


FIG. 6. Neighboring polymer sites. Two types of couplings can be distinguished here: *i*) intradimeric, which connects two sites of the same polymer (solid yellow line) and *ii*) interdimeric, which couples two sites from different polymers (blue dashed line). The distance between polymer centers (green dashed line) is assumed constant.

pressed in the second relation above and it is useful when considering static realizations in crystals. Upon the action of a unitary group $U(N)$, one has the transformations (here $\hbar = 1$)

$$p_\mu \mapsto \tilde{p}_\mu = U^\dagger p_\mu U, \quad (4)$$

$$A_\mu \mapsto \tilde{A}_\mu = U A_\mu U^\dagger - \frac{i}{g} U \partial_\mu U^\dagger, \quad (5)$$

$$|\psi\rangle \mapsto U|\psi\rangle \quad (6)$$

and they are such that $p_\mu + gA_\mu \mapsto U^\dagger(p_\mu + g\tilde{A}_\mu)U$ remains an invariant, *i.e.* the transformation of A compensates for the unitary transformation of the operators and physical states. In our discussions, this standard formulation has to be deduced in the spirit of (3): A stationary Hamiltonian formulation in first quantization necessitates a Schrödinger-like equation coming from p_0 , so a gauge invariant spectral problem involves now the transformation

$$\tilde{H} = U^\dagger H U, \quad \partial_0 U = 0 \quad (7)$$

and a static field such that

$$A_0 = \text{constant}, \quad \tilde{\mathbf{A}} = U \mathbf{A} U^\dagger - \frac{i}{g} U \nabla U^\dagger. \quad (8)$$

When it comes to derivatives on the lattice, we have to consider finite-difference operators. The aim is to identify the functional dependence of H on the field A using the correct form of minimal coupling in discrete variables. For Hamiltonians that depend of translation operators T_i and lattice vectors \mathbf{R} , we use the notation

$$\mathbf{R} = \sum_{i=1}^m n_i \mathbf{a}_i \quad (9)$$

$$N_i |n_1, \dots, n_m\rangle = n_i |n_1, \dots, n_m\rangle, \quad (10)$$

$$T_i |n_1, \dots, n_i, \dots, n_m\rangle = |n_1, \dots, n_i + 1, \dots, n_m\rangle. \quad (11)$$

where \mathbf{a}_i stand for primitive vectors and m for the number of stand vectors in the array. In our realizations, the lattice states $|n_1, \dots, n_m\rangle$ are also represented by localized wave functions around sites –e.g. a trapped mode inside a cylindrical dielectric cavity. In this language, the operators T have a differential form

$$\begin{aligned} \langle \mathbf{r} | T_i | n_1, \dots, n_2 \rangle &= \langle \mathbf{r} | n_1, \dots, n_i + 1, \dots, n_2 \rangle \\ &= \langle \mathbf{r} - \mathbf{a}_i | n_1, \dots, n_m \rangle \\ &= \exp(-i \mathbf{a}_i \cdot \mathbf{p}) \langle \mathbf{r} | n_1, \dots, n_m \rangle. \end{aligned} \quad (12)$$

It is not difficult to guess that minimal couplings should be given by complex exponentials in front of T : Indeed, under a static gauge transformation

$$\tilde{T}_i = \exp(-i \mathbf{a}_i \cdot U^\dagger \mathbf{p} U) = U^\dagger T_i U. \quad (13)$$

Moreover, a local dependence of the transformation $U(N_1, \dots, N_m) \equiv U(\mathbf{N})$ allows to write

$$\tilde{T}_i = U^\dagger(N_1, \dots, N_2) U(N_1, \dots, N_i - 1, \dots, N_m) T_i, \quad (14)$$

or $\tilde{T}_i = U^\dagger(\mathbf{N}) U(\mathbf{N} - \mathbf{e}_i) T_i$, which are the transformations we want to emulate. In order to compensate for this transformation, one writes space-dependent couplings in front of translation operator as

$$H = \sum_{k,i} \Delta_{k,i}(\mathbf{N}) (T_i)^k + \text{h.c.} + V(\mathbf{N}), \quad (15)$$

where V is a local potential, k is the range of the interaction, and $\Delta_{k,i}$ are the coupling constants as functions of site operators; in our case, they are real and positive. The aforementioned invariance imposes a transformation of Δ of the type

$$\tilde{\Delta}_{k,i}(\mathbf{N}) = \Delta_{k,i}(\mathbf{N}) U^\dagger(\mathbf{N} - \mathbf{e}_i) U(\mathbf{N}), \quad (16)$$

thus compensating the extra factors appearing in (14). If we want to know the specific dependence of H on A , the abelian case yields simply

$$\Delta_{k,i}(\mathbf{N}) = |\Delta_{k,i}(\mathbf{N})| \times \exp\{-ig \mathbf{a}_i \cdot \mathbf{A}(\mathbf{N})\}, \quad (17)$$

$$|\Delta_{k,i}(\mathbf{N})| \equiv |\Delta_{k,i}(\mathbf{N})|^\dagger. \quad (18)$$

Here, the hermitian part of Δ has been written explicitly to show that the field appears inside a unitary operator,

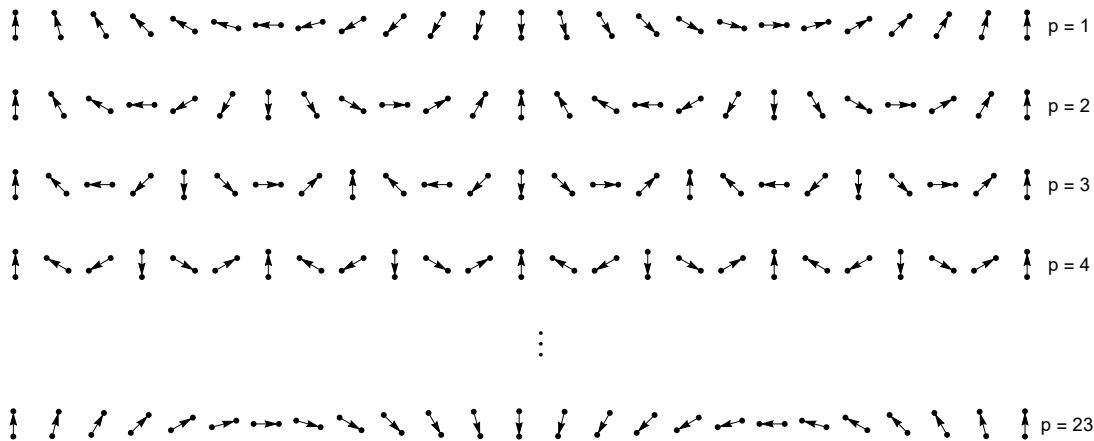


FIG. 7. Chains of rotating dimers. The arrows go from site 1 to site 2 of each dimer. The index p stands for the number of complete rotations of one dimer along the chain. This parameter is analogous to the frequency ω in Harper's Hamiltonian as shown in eq. (40) and eq. (41).

while the *modulus* is still allowed to depend on \mathbf{N} due to lattice deformations, such as those considered in [19, 35, 36]. A gauge transformation can be performed now

$$\mathbf{A}(\mathbf{N}) \mapsto \mathbf{A}(\mathbf{N}) + \frac{\hat{b}_1}{\hat{b}_1 \cdot \mathbf{a}_2} [\Phi(\mathbf{N} - \mathbf{e}_1) - \Phi(\mathbf{N})] + \frac{\hat{b}_2}{\hat{b}_2 \cdot \mathbf{a}_1} [\Phi(\mathbf{N} - \mathbf{e}_2) - \Phi(\mathbf{N})] \quad (19)$$

produces exactly the transformation (14) when substituted in (17). The unitary operator in this case is $U(\mathbf{N}) = e^{ig\Phi(\mathbf{N})}$.

For non-abelian fields, one does not express Δ directly as an exponential of A . Instead, one has to solve a relation of the type

$$U^\dagger(\mathbf{N}) \Delta_{k,i} [\tilde{\mathbf{A}}] (T_i)^k U(\mathbf{N}) = \Delta_{k,i} [\mathbf{A}] (T_i)^k \quad (20)$$

which must compensate once more (14), so now

$$U^\dagger(\mathbf{N}) \Delta_{k,i} [\tilde{\mathbf{A}}] U(\mathbf{N}) = \Delta_{k,i} [\mathbf{A}] U^\dagger(\mathbf{N} - \mathbf{e}_i) U(\mathbf{N}) \quad (21)$$

and since

$$\tilde{A}_j = U(\mathbf{N}) \left[A_j - \frac{i}{g} (1 - U^\dagger(\mathbf{N} - \mathbf{e}_j) U(\mathbf{N})) \right] U^\dagger(\mathbf{N}) \quad (22)$$

one arrives to the functional relation

$$\begin{aligned} \Delta_{k,i} \left[A_j - \frac{i}{g} (1 - \exp[-ig\Phi(\mathbf{N} - \mathbf{e}_j)]) \exp[-ig\Phi(\mathbf{N})] \right] \\ = \Delta_{k,i} [A_j] \times \exp[-ig\Phi(\mathbf{N} - \mathbf{e}_i)] \end{aligned} \quad (23)$$

at the level of A ; by defining a set of orthogonal vectors –not necessarily on the physical lattice– $\hat{b}_1 \perp \mathbf{a}_1$, $\hat{b}_2 \perp \mathbf{a}_2$, the displacement by a discretized derivative

where $\Phi = \Phi^\sigma \tau_\sigma$ is now an arbitrary non-abelian operator. This functional relation determines Δ in terms of A recursively, but its explicit solution is difficult to obtain in general. Instead we say that there is a non-trivial gauge field acting on a particle described by Hamiltonian H if there is no transformation U for which

$$\Delta_{k,i} [0] U(\mathbf{N} - \mathbf{e}_i) = U(\mathbf{N}) \Delta_{k,i} [\mathbf{A}]. \quad (24)$$

Even in the abelian case, this demands the use of non-trivial structures such as complex hopping amplitudes and, as a consequence, singular spectra via Harper's equation.

We have achieved the introduction of minimal coupling and gauge theory in the context of tight-binding systems with single-level sites, e.g. arrays of resonators. The $U(1)$ field will be implemented in section IV A with the construction of a linear chain made of dimers. This system possesses two internal degrees of freedom and the couplings Δ are modulated by the rotation of each dimer along the chain. We will show that in the appropriate basis of symmetric and antisymmetric dimeric states, two decoupled blocks emerge, both emulating singular spectra similar to those obtained from Harper's Hamiltonian. The phenomenon of wave confinement with the $SU(2)$ field is presented in section V.

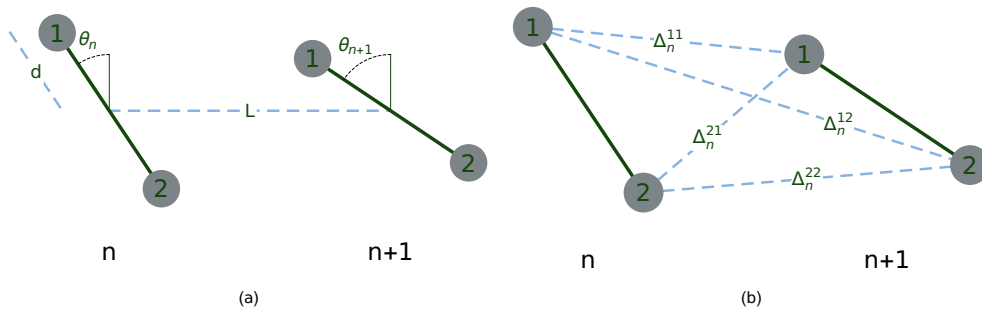


FIG. 8. (a) Geometric parameters for two adjacent dimers. (b) All pairwise inter dimer couplings. Each dimer is rotated by an angle θ_n which is a function of the number N of dimers in the chain and the number p of complete rotations of one dimer along the chain. (b) All possible pairwise couplings between sites in the same array of dimers as in (a). The couplings depend on parameters d , L and θ_n .

B. Decomposition in terms of external lattice couplings and internal polymeric couplings

The general idea to include an internal $SU(N)$ group, consists in the introduction of internal levels corresponding to each lattice site. Since one site corresponds to a single level resonator, we consider a set or cluster of such resonators put tightly together, resembling a polymer. Then, each of these sets, when regarded as a single site with a complex structure, shall have as many levels as sites in the polymer. See Fig. 6. In connection with couplings, it is also reasonable to decompose them into two parts using a diagonalization trick acting exclusively on each polymer. This helps to keep track of their contribution to the global lattice defined by the location of each polymer, or its geometric center. The distance between centers shall be associated with a coupling Δ referred to as external coupling. The distance between a geometric center and all other sites of the same polymer shall be regarded as an internal distance, therefore we refer to the corresponding Δ as internal coupling. Some triangular inequalities can be established for such couplings, as long as they are given by monotonically decreasing functions of the separation distances, e.g. exponential functions as in [37–39] or even more careful approximations involving modified Bessel functions. Based on geometric relations for the distances, we can say that the internal couplings in each polymer are more important in magnitude than the external ones. However, the external couplings shall reflect the desired crystalline structure, while internal bonds shall give rise to a local non-abelian field acting as a perturbation. Such a perturbation can be either weak or strong, depending on the geometry. Once this decomposition is achieved, we will be ready to use an appropriate basis to describe the polymeric states that interact with other neighboring polymeric states. In fact, this has a close resemblance with standard tight-binding models applied to solid state physics, where individual sites have more than one conduction orbital [40]. The diagonalization of isolated polymers does the job, eliminating thus the internal couplings between polymeric eigenstates and revealing new site-to-site interactions.

As it is evident, the number of sites in a polymer is equivalent to the dimensionality of the internal group. We note that the resulting theory is abelian, if the polymeric states are coupled only to their neighboring counterparts with the same index (*i.e.* first level with first level, second level with second level and so forth). This gives rise to a number of N decoupled abelian theories on the same lattice. On the other hand, if the polymeric states are connected with different internal eigenstate indices of a neighboring site, the corresponding Hamiltonian shall contain non-diagonal operators defined on the generating algebra $\mathfrak{su}(N)$. This shall give rise to a non-abelian theory, where the external field appears in the coupling constants instead of a local potential; this is precisely what we showed in (24).

We use the following notation: σ_{\pm} is the operator that rises (lowers) site number inside a polymer, T_i is the translation operator between neighbors in the direction of a primitive vector \mathbf{a}_i , d is the distance between the center of a polymer and one of its sites (for simplicity, we take all these as equal), L is the distance between geometric centers of neighboring polymers, and $\Delta(d_{A,B}^{m,n}) = \Delta_{A,B}^{m,n}$ is the coupling as a function of the distance as Fig. 6 shows.

IV. EMULATION OF PEIERLS SUBSTITUTION FOR $U(1)$ GAUGE FIELD

A. Linear chain

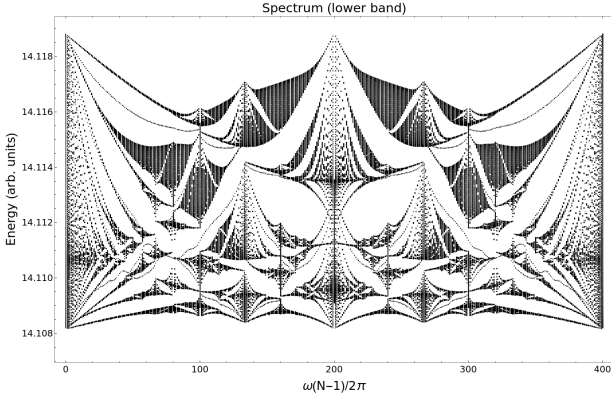
As announced in section II, we introduce the construction of dimeric chains, as can be visualized in Fig. 7. Each chain is characterized by the parameter p that corresponds to the number of complete turns of one dimer along the array. The localized states around each site are denoted by $|n, i\rangle$ where n stands for the dimer position and i is the intradimeric site. The couplings are given

by:

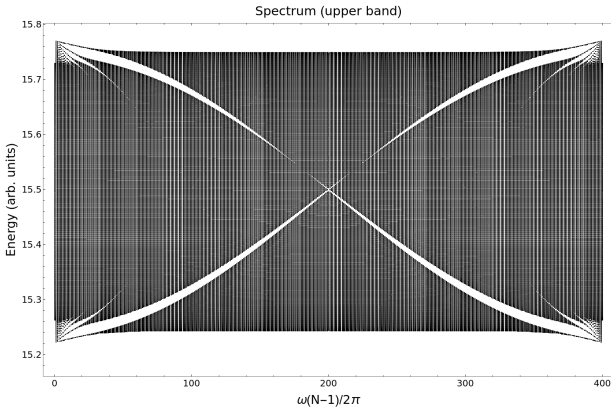
$$\begin{aligned}\Delta_{n,m}^{ij} &= \langle n, i | H | m, j \rangle \\ &= \int \psi_i^*(r) H(-\nabla^2, \mathbf{r}) \psi_j(r) dr \\ &\sim \Delta_0 \exp(-d_{n,m}^{i,j}/\lambda).\end{aligned}\quad (25)$$

where $d_{n,m}^{i,j}$ is the distance between sites (n,i) and (m,j) and λ is the evanescence length. In our description only nearest neighbors are considered. The notation for the couplings is simplified as follows: $\Delta_{n,n+1}^{ij} \mapsto \Delta_n^{i,j}$. We write the Hamiltonian of one chain as:

$$H_p = \begin{pmatrix} H_0 & h_1 & 0 & \cdots & 0 \\ h_1^\dagger & H_0 & h_2 & \ddots & 0 \\ 0 & h_2^\dagger & H_0 & & 0 \\ \vdots & \ddots & & \ddots & 0 \\ 0 & & & & H_0 & h_{n-1} \\ 0 & & 0 & h_{n-1}^\dagger & H_0 \end{pmatrix}, \quad (26)$$



(a)



(b)

FIG. 9. Deformed fractal spectrum due to off-diagonal couplings produced by an $SU(2)$ field. (a) Strong corrections to the symmetric mode band. (b) Mild corrections to the anti-symmetric mode band.

where

$$H_0 = \begin{pmatrix} 0 & \Delta_0 \\ \Delta_0 & 0 \end{pmatrix}, \quad h_n = \begin{pmatrix} \Delta_n^{11} & \Delta_n^{12} \\ \Delta_n^{21} & \Delta_n^{22} \end{pmatrix}. \quad (27)$$

In this notation, H_0 represents the Hamiltonian of one dimer with its on-site energies shifted to zero for simplicity. Now we can diagonalize each dimeric block in the main diagonal using a Hadamard matrix:

$$H_p^{(1)} = (\mathbf{1}_N \otimes U)^\dagger H_p (\mathbf{1}_N \otimes U), \quad U = \frac{1}{\sqrt{2}} \begin{pmatrix} +1 & +1 \\ +1 & -1 \end{pmatrix}. \quad (28)$$

The transformed Hamiltonian in the symmetric and antisymmetric basis is:

$$H_p^{(1)} = \begin{pmatrix} H_D & \tilde{h}_1 & 0 & \cdots & 0 \\ \tilde{h}_1^\dagger & H_D & \tilde{h}_2 & \ddots & 0 \\ 0 & \tilde{h}_2^\dagger & H_D & & 0 \\ \vdots & \ddots & & \ddots & 0 \\ 0 & & & & H_D & \tilde{h}_{n-1} \\ 0 & & 0 & \tilde{h}_{n-1}^\dagger & H_D \end{pmatrix}, \quad (29)$$

with H_D and \tilde{h}_i given by:

$$H_D = \begin{pmatrix} \Delta_0 & 0 \\ 0 & -\Delta_0 \end{pmatrix}, \quad \tilde{h}_n = \begin{pmatrix} \Delta_n^{AA} & \Delta_n^{AS} \\ \Delta_n^{SA} & \Delta_n^{SS} \end{pmatrix}. \quad (30)$$

The superscript of Δ_n in \tilde{h}_n now represents the couplings between antisymmetric (A) and symmetric (S) states. We express $\Delta_n^{AA}, \Delta_n^{SA}, \Delta_n^{AS}$ and Δ_n^{SS} in terms of site-to-site couplings:

$$\begin{aligned}\Delta_n^{AA} &= \frac{1}{2} (\Delta_n^{11} + \Delta_n^{12} + \Delta_n^{21} + \Delta_n^{22}) \\ \Delta_n^{AS} &= \frac{1}{2} (\Delta_n^{11} - \Delta_n^{12} + \Delta_n^{21} - \Delta_n^{22}) \\ \Delta_n^{SA} &= \frac{1}{2} (\Delta_n^{11} + \Delta_n^{12} - \Delta_n^{21} - \Delta_n^{22}) \\ \Delta_n^{SS} &= \frac{1}{2} (\Delta_n^{11} - \Delta_n^{12} - \Delta_n^{21} + \Delta_n^{22}).\end{aligned}\quad (31)$$

Reorganization of the transformed Hamiltonian $H_p^{(1)}$ into A and S blocks obtains

$$H_p^{(2)} = \begin{pmatrix} H_A & \delta_{AS} \\ \delta_{AS}^\dagger & H_S \end{pmatrix}, \quad (32)$$

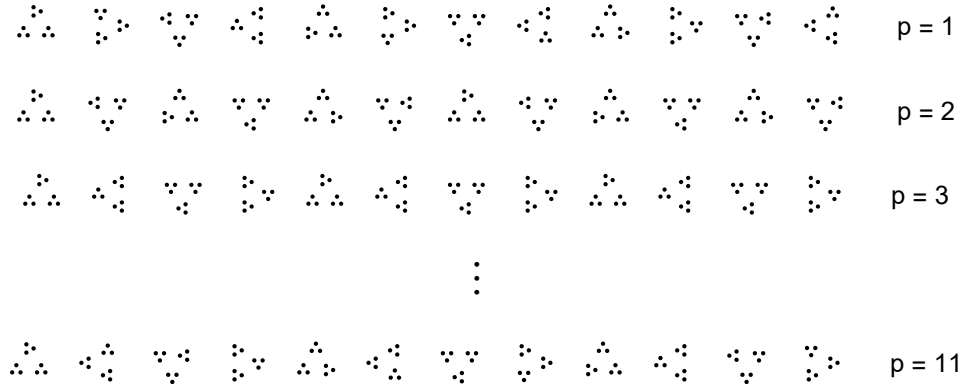


FIG. 10. Linear chains made of trimers. The unit cell rotates a number p of complete turns along the chain. The global C_3 symmetry is broken if one internal trimer is rotated with respect to the other two. When the symmetry C_3 is restored a flat band appears in the inferior part of the spectrum. This symmetry breaking splits the resulting energy bands.

where H_A and H_S contain only A–A and S–S couplings respectively:

$$H_A = \begin{pmatrix} \Delta_0 & \Delta_1^{AA} & 0 & \dots & 0 \\ \Delta_1^{AA} & \Delta_0 & \Delta_2^{AA} & \ddots & \vdots \\ 0 & \Delta_2^{AA} & \Delta_0 & & \\ \vdots & \ddots & & \ddots & \\ 0 & & & \Delta_0 & \Delta_{n-1}^{AA} \\ & & & \Delta_{n-1}^{AA} & \Delta_0 \end{pmatrix} \quad (33)$$

$$H_S = \begin{pmatrix} \Delta_0 & \Delta_1^{SS} & 0 & \dots & 0 \\ \Delta_1^{SS} & \Delta_0 & \Delta_2^{SS} & \ddots & \vdots \\ 0 & \Delta_2^{SS} & \Delta_0 & & \\ \vdots & \ddots & & \ddots & \\ 0 & & & \Delta_0 & \Delta_{n-1}^{SS} \\ & & & \Delta_{n-1}^{SS} & \Delta_0 \end{pmatrix} \quad (34)$$

$$\delta_{AS} = \begin{pmatrix} 0 & \Delta_1^{AS} & 0 & \dots & 0 \\ \Delta_1^{SA} & 0 & \Delta_2^{AS} & \ddots & \vdots \\ 0 & \Delta_2^{SA} & 0 & & \\ \vdots & \ddots & & \ddots & \\ 0 & & & 0 & \Delta_{n-1}^{AS} \\ & & & \Delta_{n-1}^{SA} & 0 \end{pmatrix} \quad (35)$$

We observe from (31) that the elements of δ_{AS} depend on the couplings between neighboring sites, and this dependence is purely geometrical due to the definition of $\Delta_{n,m}^{ij}$ in (25). The ideal case was announced in section II where δ_{AS} is identically zero; the corresponding spectrum is illustrated in Fig. 1.

In general, the Hamiltonian $H_p^{(2)}$ possesses two coupled blocks, although some approximations can be made. If the elements of δ_{AS} are smaller than the ones of H_A and H_S , the spectrum consists of decoupled bands with a Cantor spectrum; in the more general case, the Hofstadter butterfly appears slightly deformed, as the reader may visualize in Fig. 9.

In order to obtain the couplings as functions of site

number, we must calculate the four distances between the dimer n and the dimer $n+1$. Let us denote by $\mathbf{r}_n^{(i)}$, $i = 1, 2$ the position vector of site i in dimer n , so all the pairwise distances are given by the following expression:

$$d_n^{ij} = |\mathbf{r}_n^{(i)} - \mathbf{r}_{n+1}^{(j)}| = L \{1 + 2\alpha^2 A_n^{ij} - 2\alpha B_n^{ij}\}^{1/2}, \quad (36)$$

where A_n^{ij} and B_n^{ij} contain information on the rotations of each dimer $\theta_n = 2\pi P(n-1)/(N-1)$ as

$$\begin{aligned} A_n^{ij} &= 1 - (-1)^{i+j} \cos(\theta_n - \theta_{n+1}) \\ B_n^{ij} &= (-1)^i \sin \theta_n - (-1)^j \sin \theta_{n+1}, \end{aligned} \quad (37)$$

and $\alpha = d/L$. The corresponding couplings are given as follows:

$$\Delta_n^{ij} \simeq \left\{ 1 + B_n^{ij} \frac{d\alpha}{\lambda} + \left[\frac{B_n^{ij^2}}{2} \left(1 + \frac{L}{\lambda} \right) - A_n^{ij} \right] \frac{d\alpha^2}{\lambda} \right\} \Delta_L. \quad (38)$$

where a second order approximation for $\alpha \ll 1$ has been used and $\Delta_L = \Delta_0 \exp(-L/\lambda)$. From (31) the second order approximation in α leads to

$$\Delta_n^{SS} = \frac{2d^2}{\lambda L} \left\{ \cos \theta_n \cos \theta_{n+1} - \frac{L}{\lambda} \sin \theta_n \sin \theta_{n+1} \right\} \Delta_L. \quad (39)$$

In the special case when $L/\lambda = 1$, we obtain

$$\Delta_n^{SS} = \frac{2d^2}{L^2} \cos[\omega(2n-1)] \Delta_L, \quad (40)$$

with the angular frequency ω defined as $2\pi p/(N-1)$. It can be demonstrated that there is a unitary map between the Harper's Hamiltonian and a tight-binding model without potential and with site-dependent couplings, as obtained in (40). This rigorous map is of utmost importance, and it is included in Appendix A. The

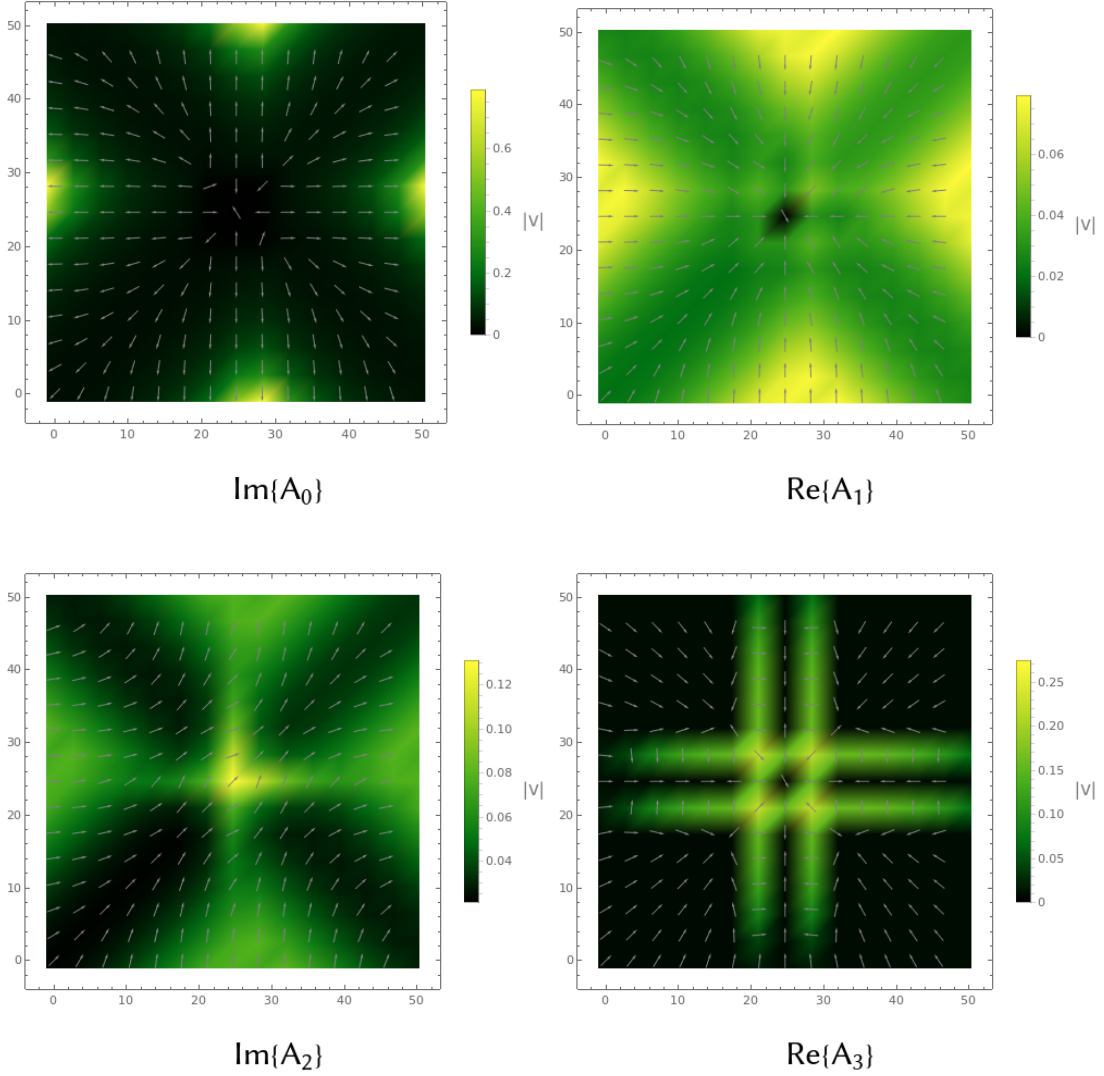


FIG. 11. Portraits of \mathbf{A} on the square lattice. The components $\text{Im}\{A_0\}$ and $\text{Im}\{A_2\}$ are presented, as $\text{Re}\{A_0\} = \text{Re}\{A_2\} = 0$. Similarly the components $\text{Re}\{A_1\}$ and $\text{Re}\{A_3\}$ are presented, while $\text{Im}\{A_1\} = \text{Im}\{A_3\} = 0$.

effective parameter is $\Lambda = 1$ for the symmetric mode band. On the other hand, for Δ_n^{AA} couplings we have:

$$\Delta_n^{AA} = 2\gamma \left\{ 1 - \frac{\beta\alpha^2(\beta+1)}{\gamma} \cos\omega \cos[\omega(2n-1)] \right\} \Delta_L. \quad (41)$$

where

$$\begin{aligned} \gamma &= 2 + \beta\alpha^2(\beta-1), \\ \beta &= \frac{d}{\lambda}, \quad \alpha = \frac{L}{d}. \end{aligned} \quad (42)$$

In this case, Λ in the Harper's model must be assumed small as shown in (A16). The estimated effective is $\Lambda = 0.08 \cos\omega$ for the antisymmetric mode band. It is worth noting the non-removable frequency dependence of Λ . The Lebesgue measure for the AMO is $|4 - 4\Lambda|$ [41]. The symmetric and antisymmetric bands have zero and $3.68|\cos\omega|$ Lebesgue measure respectively.

A more general treatment to find the couplings as functions of site numbers, consists in a decomposition of \tilde{h}_n in polar form:

$$\begin{aligned} \tilde{h}_n &= UP = \exp(i\sigma_2\phi)P \\ &= \begin{pmatrix} \cos\phi & \sin\phi \\ -\sin\phi & \cos\phi \end{pmatrix} \begin{pmatrix} e^\theta \cosh\chi & \sinh\chi \\ \sinh\chi & e^{-\theta} \cosh\chi \end{pmatrix}, \end{aligned} \quad (43)$$

obtaining thus the following relations

$$\begin{aligned} \Delta_n^{AA} &= e^\theta \cos\phi \cosh\chi + \sin\phi \sinh\chi \\ \Delta_n^{AS} &= e^{-\theta} \sin\phi \cosh\chi + \cos\phi \sinh\chi \\ \Delta_n^{SA} &= -e^\theta \sin\phi \cosh\chi + \cos\phi \sinh\chi \\ \Delta_n^{SS} &= e^{-\theta} \cos\phi \cosh\chi - \sin\phi \sinh\chi. \end{aligned} \quad (44)$$

where the parameters χ , ϕ and θ are given in terms of

the couplings as:

$$e^\theta \cosh \chi = \frac{2(\Delta_n^{11} \Delta_n^{12} + \Delta_n^{21} \Delta_n^{22}) + \gamma}{2\gamma^{1/2}}, \quad (45)$$

$$e^{-\theta} \cosh \chi = \frac{-2(\Delta_n^{11} \Delta_n^{12} + \Delta_n^{21} \Delta_n^{22}) + \gamma}{2\gamma^{1/2}}, \quad (46)$$

$$\gamma = (\Delta_n^{12} - \Delta_n^{21})^2 + (\Delta_n^{11} + \Delta_n^{22})^2. \quad (47)$$

We have seen how to obtain a Hamiltonian equivalent to Harper's model in an abelian sector of the theory. As presented in previous sections, this produces indeed a butterfly coming from an AMO.

On the other hand, non-negligible elements in δ_{SA} reveal the non-abelian nature of the field as we shall explore in the next section.

V. EMULATION OF SU(2) FIELD

The present section shows that the geometric dependence of couplings can be decomposed into a function of the distance between dimer centers and a function of each dimer orientation. The latter dependence is crucial in the construction of arrays with localized wave functions as the one presented in section V C.

A. A model with SU(2)

Following the general formalism exposed in sections III A and III B, we study the construction of a square lattice made of dimers. We define the projectors $P_\pm = (1 \pm \sigma_3)/2$ that select the state 1 or 2 inside one dimer. The coupling between state 1 of a lattice site with state 2 belonging to its neighbor at the right would correspond to the operator $T_1 \sigma_+$ and its hermitian conjugate, by reciprocity. A square lattice with nearest lattice couplings, internal dimer couplings and arbitrary on-site energies is

TABLE I. Fractal dimensions of the symmetric mode band.

$\omega 2\pi / (N - 1)$	Fractal dimension
0	0.9606
1	0.9601
2	0.4980
3	0.4884
5	0.4244
7	0.6525
11	0.6848
13	0.6995
17	0.6941
19	0.7010
23	0.7233
29	0.6897
31	0.7308
37	0.7516
41	0.7389

described by the following Hamiltonian

$$\begin{aligned} H = & (\Delta_1^+ \sigma_+ + \Delta_1^- \sigma_- + \tilde{\Delta}_1^+ P_+ + \tilde{\Delta}_1^- P_-) T_1 + h.c. \\ & + (\Delta_2^+ \sigma_+ + \Delta_2^- \sigma_- + \tilde{\Delta}_2^+ P_+ + \tilde{\Delta}_2^- P_-) T_2 + h.c. \\ & + \Delta_0^+ \sigma_+ + \Delta_0^- \sigma_- + \tilde{\Delta}_0^+ P_+ + \tilde{\Delta}_0^- P_- + V \end{aligned} \quad (48)$$

whereas a triangular lattice (which has coordination number 6) made of dimeric sites has a Hamiltonian

$$\begin{aligned} H = & ((\Delta_1^+ \sigma_+ + \Delta_1^- \sigma_- + \tilde{\Delta}_1^+ P_+ + \tilde{\Delta}_1^- P_-) T_1 + h.c. \\ & + (\Delta_2^+ \sigma_+ + \Delta_2^- \sigma_- + \tilde{\Delta}_2^+ P_+ + \tilde{\Delta}_2^- P_-) T_2 + h.c. \\ & + (\Delta_3^+ \sigma_+ + \Delta_3^- \sigma_- + \tilde{\Delta}_3^+ P_+ + \tilde{\Delta}_3^- P_-) T_2^\dagger T_1 + h.c. \\ & + \Delta_0^+ \sigma_+ + \Delta_0^- \sigma_- + \tilde{\Delta}_0^+ P_+ + \tilde{\Delta}_0^- P_- + V \end{aligned} \quad (49)$$

where T_3 is actually $T_2^\dagger T_1$. The six neighbors are obtained here if we recognize that the hermitian conjugate of the third row reverses the sign of the vector $\mathbf{a}_1 - \mathbf{a}_2$. The Hamiltonian of a particle in a nearest neighbor lattice of coordination number c can be written in the same fashion. Moreover, we choose to express σ_\pm in terms of $\sigma_{1,2}$, P_\pm in terms of σ_3 and $\sigma_0 = \mathbf{1}$. The resulting expression is refreshingly simple if we adopt the Einstein convention for greek indices in σ_μ , *i.e.*

$$H = \sum_{k=1}^c \Delta_k^\mu \sigma_\mu T_k + \Delta_0^\mu \sigma_\mu + h.c., \quad (50)$$

albeit no Lorentzian metric has been required for this theory.

If the operators Δ_k^μ representing local-dependent couplings are all parallel, then $\Delta_k^\mu = \Delta^\mu$ for all j , and the Hamiltonian (50) will represent a lattice with site-dependent deformations but without a gauge field. We have the following factorization property:

$$H = \Delta^\mu \sigma_\mu \sum_{k=1}^c T_k + h.c. + \Delta_0^\mu \sigma_\mu \quad (51)$$

Another case of reduction is the decoupling of identical lattices, *i.e.* $\Delta_k^1 = \Delta_k^2 = \Delta_k^3 = 0$ for all k , leading to

$$H = \mathbf{1} \otimes \left\{ \sum_k \Delta_k^0 T_k + h.c. + V \right\}, \quad (52)$$

i.e. a theory without internal structure. It is important to note that in (50), the coupling constants are complex in general; however, in specific realizations, the use of real and positive Δ_k^\pm for each site shall impose some restrictions on the values of Δ_k^μ . Evidently, the result is aperiodic in general, as described in Fig. 7.

Before diagonalizing each dimer, we decompose each site-to-site coupling in center-to-center couplings plus fluctuations:

$$\Delta_k^\mu(d_{n,m}^{i,j}) = \Delta(L) + \delta_k^\mu(d_{n,m}^{i,j}) \quad (53)$$

The distances $d_n^{i,j}$ explained in Fig. 8, can be expressed in terms of reference lengths L, d and the angles θ_n, θ_{n+1} ,

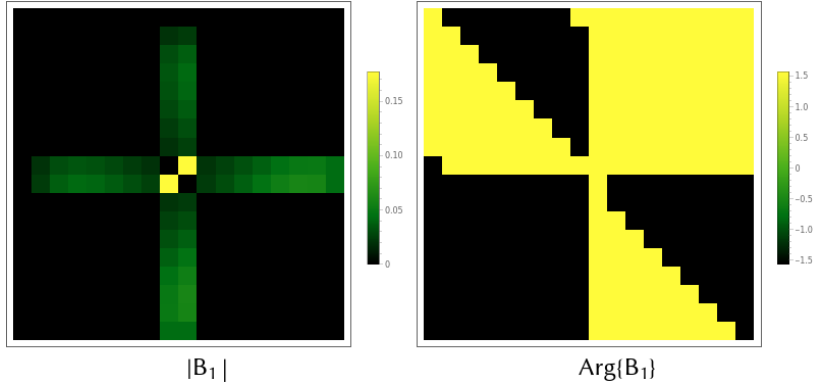


FIG. 12. Component σ_1 of the field B_z . This field is the result of the commutator $[A_x, A_y]$ in eq. (59) and constitutes the purely non-abelian contribution of the field. The other components of B_z are small in comparison.

such that the dependence of δ_k^μ on such parameters can be exhibited. Assuming only orientational dependence but no deformation, and the fact that Δ must be real and positive, one has $\Delta_k^3 = \Delta_k^2 = 0$, uniform on-site energies (*i.e.* $V = 0$ can be imposed) and the Hamiltonian becomes

$$H = (\mathbf{1} + \sigma_1)\Delta(L)\sum_k T_k + h.c. + \sum_k \delta_k^\mu \sigma_\mu T_k + h.c. + \Delta(d)\sigma_1, \quad (54)$$

where the first term represents the periodic lattice, the second term contains all orientational fluctuations (disorder could be introduced in this part) and the last term is the intra-dimer coupling contribution. Finally, we intro-

duce a change of basis, in order to transform each dimer into an effective two-level potential well. It suffices to diagonalize σ_1 , leading to the following Hamiltonian:

$$\begin{aligned} \tilde{H} = P_+ & \left\{ \sum_k (\Delta(L) + \delta_k^1 + \delta_k^0)T_k + h.c. + \Delta(d) \right\} \\ & + P_+ \left\{ \sum_k (\delta_k^0 - \delta_k^1)T_k + h.c. - \Delta(d) \right\} \\ & + \sigma_1 \sum_k \delta_k^3 (T_k + T_k^\dagger) \end{aligned} \quad (55)$$

or in block form

$$\tilde{H} = \begin{pmatrix} \sum_k (\Delta(L) + \delta_k^1 + \delta_k^0)T_k + h.c. + \Delta(d) & \sum_j \delta_k^3 (T_k + T_k^\dagger) \\ \sum_k \delta_k^3 (T_k + T_k^\dagger) & \sum_k (\delta_k^0 - \delta_k^1)T_k + h.c. - \Delta(d) \end{pmatrix} \quad (56)$$

where each block is a Hamiltonian for the global lattice. The off-diagonal blocks represent the non-abelian nature of the resulting theory, in the basis of dimer eigenfunctions. The fact that this dependence cannot be removed, indicates that the emulation of interactions with an external non-abelian field depend crucially on the orientational fluctuations δ_k^1, δ_k^3 , which in turn can be geometrically designed as indicated in Fig. 7.

By comparing the Hamiltonians (56) and (32) we can conclude that the non-abelian behavior of the field is originated by the dimer orientations of the chains.

B. Effective negative couplings and level inversion revisited

When the fluctuations are small, we may try to find an approximate representation that eliminates the off-diagonal blocks. Here, we must recover an abelian gauge

field, but by the same token, this field must be described by the fluctuations in the orientations. If we simply eliminate δ_j^3 , the second block has a peculiarity already noted in [42, 43]: level inversion can be achieved whenever $\delta_j^0 < \delta_j^1$, and even a degeneracy point occurs when $\delta_j^0 = \delta_j^1$, *i.e.* a hidden symmetry that does not pertain to the underlying lattice symmetries. The level inversion corresponds to the realization of negative couplings using exclusively positive on-site waves. Another way to look at this, according to [42], is to recognize that the basis of a dimer contains both symmetric and antisymmetric functions, which means that couplings between dimeric excited states can change sign if the antisymmetric waves enter with opposite signs in the overlap integrals.

In the case where the fluctuations are indeed small, but their effect is not completely neglected to second order, a perturbative approach can help to reabsorb them in the diagonal part by a unitary transformation.

C. Wave confinement in SU(2). Bound states

In section II we showed examples of lattices that exhibit the confinement phenomenon of its wave function in the center of the array. In this section we present the construction of the corresponding square lattice.

Our method of construction is based on the intensities of the couplings between two adjacent dimers in the direction of the primitive vectors. The strongest couplings must be located at the center of the array while the orientation of the dimers out of this region must be disposed in a configuration that favors small coupling values. We achieve these conditions with four central dimers illustrated in Fig. 3. In general, the position of each site is given by the following expressions:

$$\mathbf{a}_1^{(\mathbf{n})} = \left((n_x - 1)l - d \sin \left[\frac{\pi}{4} + \frac{\pi}{2(n-2)} \right] (n_y - n_x), -(n_y - 1)l - d \cos \left[\frac{\pi}{4} + \frac{\pi}{2(n-2)} \right] (n_y - n_x) \right) \quad (57)$$

$$\mathbf{a}_2^{(\mathbf{n})} = \left((n_x - 1)l - d \sin \left[\frac{5\pi}{4} + \frac{\pi}{2(n-2)} \right] (n_y - n_x), -(n_y - 1)l - d \cos \left[\frac{5\pi}{4} + \frac{\pi}{2(n-2)} \right] (n_y - n_x) \right), \quad (58)$$

where $\mathbf{a}_1^{(\mathbf{n})}$ and $\mathbf{a}_2^{(\mathbf{n})}$ stand for the positions 1 and 2 of the dimer at $\mathbf{n} = (n_x, n_y)$. Now we vary the lattice parameter and find a localized state at the top of the energy band. This localized state moves downwards, as the lattice constant increases with fixed dimeric distance. In fact, it merges with the propagation band in the limit of negligible intradimeric distance—small compared to the lattice constant—and reveals the non abelian nature of the effect. An analogy with solitons can be made here, as the localized state dwells in a region produced by a Hedgehog-type external field. This configuration of dimers has some characteristics in common with solutions of the classical non-linear field equations possessing a finite energy and localized non-dispersive energy density *i.e.* this wave travels with its shape unchanged[44, 45]. Moreover, such solution falls to zero at infinity. In the non-linear theory we pretend to emulate, the solutions perturb our discrete Schrödinger equation.

The portrait of the wave function for the higher energy state was shown in section 3 in Fig. 4. We observe that the electronic state is confined at the center of the array, but we are also interested in the shape of the emulated non-abelian field. In the direction perpendicular to the lattice plane, B_z is obtained as follows:

$$B_z = \partial_y A_x - \partial_x A_y - i[A_x, A_y], \quad (59)$$

where the commutator plays here an important role. In

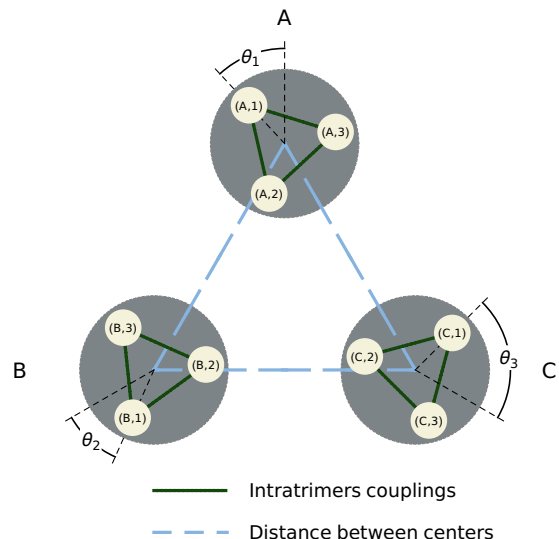


FIG. 13. Unit cell for the chain of trimers. Each internal triangle can rotate independently with angles θ_1 , θ_2 and θ_3 . The dashed blue lines represent the distances between centers.

order to calculate the components of A , first we must express each 2×2 coupling block as an exponential:

$$\Delta(\mathbf{N}) = \exp(\Phi^{(0)} \mathbf{1} + \Phi \cdot \sigma). \quad (60)$$

The component A_i is the difference between $\Phi(\mathbf{N})$ and $\Phi(\mathbf{N} - \hat{\mathbf{e}}_i)$. The projections on the Pauli basis $\sigma_0, \sigma_1, \sigma_2$ and σ_3 of \mathbf{A} are readily found by computing $\text{Tr}(A\sigma_i)$ and are illustrated in Fig 11. The real part of $A^{(0)}$, $A^{(2)}$ and the imaginary part of $A^{(1)}$, $A^{(3)}$ are zero.

VI. BAND MIXING IN SU(3) MODELS WITH COLOR

The emulation of SU(3) fields can be performed in a similar way as presented for the previous SU(2) case. This time we construct a linear chain made of trimers, where the unit cell is shown in Fig. 13. The energy levels of each internal trimer represent three internal degrees of freedom in the cell. As the triangles rotate independently with angles θ_1, θ_2 and θ_3 , we can break or restore the local polygonal symmetry of each cell, and thus manipulate the emergent band structure. When these angles vanish, the system has $C_3 \times C_3$ symmetry. The Hamiltonian of

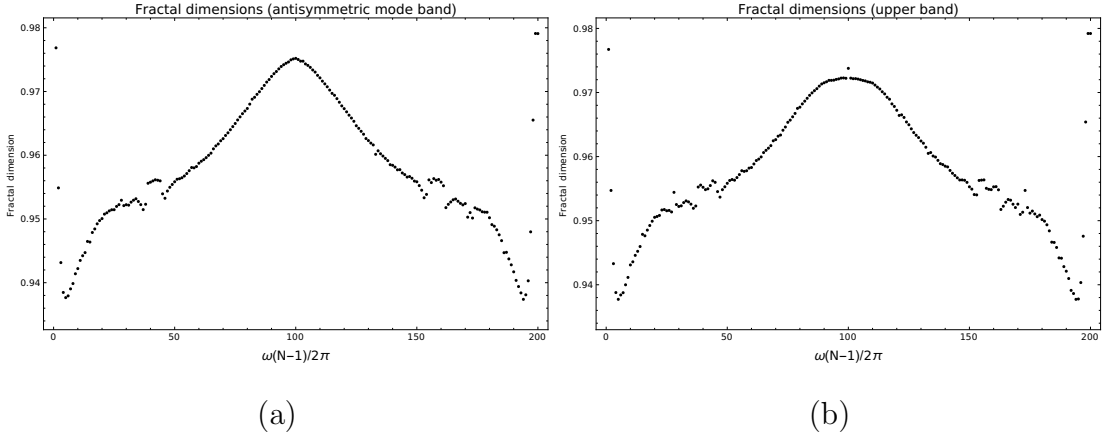


FIG. 14. Panels (a) and (b) present the fractal dimensions of the antisymmetric mode band and upper band respectively. Both spectra show similarities in the fractal dimension values.

the array is, in matrix form:

$$H = \begin{pmatrix} H_0 & \Delta_{AB} & \Delta_{AC} \\ \Delta_{AB}^\dagger & H_0 & \Delta_{BC} \\ \Delta_{AC}^\dagger & \Delta_{BC}^\dagger & H_0 \end{pmatrix}, \quad (61)$$

$$H_0 = \begin{pmatrix} E & \Delta & \Delta \\ \Delta & E & \Delta \\ \Delta & \Delta & E \end{pmatrix}, \quad (62)$$

$$\Delta_{mn} = \begin{pmatrix} \Delta_{m1,n1} & \Delta_{m1,n2} & \Delta_{m1,n3} \\ \Delta_{m2,n1} & \Delta_{m2,n2} & \Delta_{m2,n3} \\ \Delta_{m3,n1} & \Delta_{m3,n2} & \Delta_{m3,n3} \end{pmatrix}, \quad (63)$$

where $m, n = A, B, C$ and $\Delta_{ml,nk}$ is the coupling between the l -th site of the trimer m with the k -th site of trimer

n . A transformed Hamiltonian is obtained if we use the 3×3 matrix that diagonalizes H_0 , i.e. $\tilde{H} = U^\dagger H_0 U$ where $U = \mathbf{1} \otimes U_{3 \times 3}$. The transformed matrix elements are calculated analytically below:

$$(U_{3 \times 3})_{p,q} = \frac{1}{\sqrt{3}} \exp \left[\frac{i2\pi}{3} (2+p)q \right], \quad (64)$$

$$(\tilde{\Delta}_{mn})_{pq} = \frac{e^{4\pi i(q-p)/3}}{3} \sum_{k,k'=1}^3 e^{2\pi i(k'q-kp)/3} \Delta_{mk,nk'}. \quad (65)$$

Now, the Hamiltonian is expressed in the eigenbasis of C_3 : Reorganizing matrix elements leads to a Hamiltonian divided into three blocks:

$$H = \begin{pmatrix} S_1 & (\Delta'_{AB})_{33} & (\Delta'_{AC})_{33} & 0 & (\Delta'_{AB})_{31} & (\Delta'_{AC})_{31} & 0 & (\Delta'_{AB})_{32} & (\Delta'_{AC})_{32} \\ (\Delta'_{AB})_{33}^* & S_2 & (\Delta'_{BC})_{33} & (\Delta'_{AC})_{13}^* & 0 & (\Delta'_{BC})_{31} & (\Delta'_{AC})_{23}^* & 0 & (\Delta'_{BC})_{32} \\ (\Delta'_{AC})_{33}^* & (\Delta'_{BC})_{33}^* & S_3 & (\Delta'_{AC})_{13}^* & (\Delta'_{BC})_{13}^* & 0 & (\Delta'_{AC})_{23}^* & (\Delta'_{BC})_{23}^* & 0 \\ 0 & (\Delta'_{AB})_{13} & (\Delta'_{AC})_{13} & D_{11} & (\Delta'_{AB})_{11} & (\Delta'_{AC})_{11} & 0 & (\Delta'_{AB})_{12} & (\Delta'_{AC})_{12} \\ (\Delta'_{AB})_{31}^* & 0 & (\Delta'_{BC})_{13} & (\Delta'_{AB})_{11}^* & D_{21} & (\Delta'_{BC})_{11}^* & (\Delta'_{AB})_{21}^* & 0 & (\Delta'_{BC})_{12} \\ (\Delta'_{AC})_{31}^* & (\Delta'_{BC})_{31}^* & 0 & (\Delta'_{AC})_{11}^* & (\Delta'_{BC})_{11}^* & D_{31} & (\Delta'_{AC})_{21}^* & (\Delta'_{BC})_{21}^* & 0 \\ 0 & (\Delta'_{AB})_{23} & (\Delta'_{AC})_{23} & 0 & (\Delta'_{AB})_{21} & (\Delta'_{AC})_{21} & D_{12} & (\Delta'_{AB})_{22} & (\Delta'_{AC})_{22} \\ (\Delta'_{AB})_{32}^* & 0 & (\Delta'_{BC})_{23} & (\Delta'_{AB})_{12}^* & 0 & (\Delta'_{BC})_{21} & (\Delta'_{AB})_{22}^* & D_{22} & (\Delta'_{BC})_{22} \\ (\Delta'_{AC})_{32}^* & (\Delta'_{BC})_{32}^* & 0 & (\Delta'_{AC})_{12}^* & (\Delta'_{BC})_{12}^* & 0 & (\Delta'_{AC})_{22}^* & (\Delta'_{BC})_{22}^* & D_{32} \end{pmatrix}. \quad (66)$$

The symmetry breaking of a global C_3 of each trimer is introduced by a rotation of only one of the internal dimers; as a consequence, triple degeneracy points emerge as announced previously. Note though that doublets are never split. The internal C_3 breaking is achieved by deformation of the internal trimers, and in this case lifted doublets appear. Following the same path as in the case of $SU(2)$, we construct a linear chain made of rotated unit cells. This system produces the spectrum of the Fig. 5 where we find overlapped bands. The superior band contains nine copies of the Hofstadter butterfly.

The model shows emergent flat bands, of potential interest in recent studies on superconductors.

Finally, the model can be generalized also to a 2D lattice, in a similar way to the $SU(2)$ case, with the aim of emulating confinement due to $SU(3)$ color fields.

VII. CONCLUSION

In this work, the emulation of non abelian fields was studied in periodic, quasi-periodic and defective lattices

with internal degrees of freedom given by the energy levels of a polymer. The full lattice is homogeneous, i.e. all sites were identical. For a given set of geometric parameters in a linear chain of rotating dimers, the projections of the energy levels in the uncoupled symmetric and anti-symmetric states reproduced well Harper's Hamiltonian spectra with $\Lambda = 1.7$ and $\Lambda = 1$ for the two emergent bands. It was also possible to show that the spectrum was independent of Bloch' quasimomentum, as in the standard theory of ergodic operators. This gave us a clear indication of an emergent magnetic field produced by mere deformations.

In the general description of coupled bands, the orientations of the couplings between neighboring sites were responsible for non zero elements in the diagonal block of the Hamiltonian; this showed that our construction was a genuine realization of a non-abelian theory in a regime of strong couplings between bands. The phenomenon of confinement due to $SU(2)$, was emulated in a square array with dimers where the hopping amplitudes were tuned in order to produce an effective (non-diagonal) defect; the wave function as shown to be located at the center of the crystal and its energy was found on the superior part of the propagation band. This localized state merged with the latter, as the lattice constant increased, which resulted in a fully periodic array in the limit of negligible dimer size. It is important to note that the dimeric structure could be shown to be indispensable to determine whether a non-abelian group $SU(2)$ entered or not in the description. The bound state located at the lattice defect would simply disappear in the absence of a non-abelian theory.

A few words are in order in connection with technological applications. The magnetic field emulated with deformations allows to study similar effects in mesoscopic systems and wave transport. Its applications to wave propagation in elastic tight-binding emulations [46] and photonic crystals offers itself as a type of metallic-to-insulator transition in systems where external fields that manipulate waves are not available. We have also shown that the introduction of extra orbitals in solid state physics leads to deformations of Cantor sets. As an outlook, we plan to analyze the implications of such spectral deformations on the Quantum Hall effect [47, 48], whose mysteries are yet to be fully explained.

ACKNOWLEDGMENTS

Beca 291197 CONACYT and project 100518931-VIEP BUAP-CA-289.

Appendix A: Unitary map between translation operators in 1D; beyond Aubry's duality.

In this section we show explicitly the unitary map of the Harper Hamiltonian into a tight-binding opera-

tor without potential, but with variable couplings. For ease in the calculations, we shall work in a representation where the transformation an site number operators act on smooth functions, i.e. $T \rightarrow e^{iap}$, $p = -i\hbar\partial_x$, $N \rightarrow x/a$. If we act on a complete basis of Wannier functions $\phi_b(x-a)$ this represents no loss of generality. However, we must make sure that our unitary map takes us from periodic functions (period a , index band b) to periodic functions. Let us take the following unitary transformation on the Hamiltonian

$$\tilde{H} = UHU^\dagger, \quad UU^\dagger = \mathbf{1}. \quad (\text{A1})$$

The unitary operator U can be expressed as:

$$U = V(N) \exp\{i(\alpha p^2 + \beta p)\}, \quad (\text{A2})$$

such that $V(N)V^\dagger(N) = \mathbf{1}$, $\alpha, \beta \in \mathcal{R}$. We shall see that U does not change the nature of the lattice if α and β are properly chosen. We have

$$T = e^{iap}, \quad E \equiv e^{i\omega N} = e^{i\omega x/a} \quad (\text{A3})$$

and defining $v \equiv \omega/a$, E can be written as $E \equiv e^{ivx}$, where $x = i\hbar\partial_p$. With these definitions, the Harper's Hamiltonian (Almost Mathieu Operator) has the form:

$$H = T + T^\dagger + \Lambda(E + E^\dagger), \quad (\text{A4})$$

for $\nu = 0$, which is isospectral to any $\nu \neq 0$. Direct substitution leads to

$$\begin{aligned} UTU^\dagger &= V(N)e^{i(\alpha p^2 + \beta p)}Te^{-i(\alpha p^2 + \beta p)}V^\dagger(N) \\ &= V(N)TV^\dagger(N) = V(x/a)TV^\dagger(x/a) \\ &= V(N)V^\dagger(N+1)T. \end{aligned} \quad (\text{A5})$$

In addition

$$UEU^\dagger = V(N)e^{i(\alpha p^2 + \beta p)}Ee^{-i(\alpha p^2 + \beta p)}V^\dagger(N) \quad (\text{A6})$$

and

$$Ef(p) = f(p-v)E, \quad (\text{A7})$$

so that

$$\begin{aligned} UEU^\dagger &= V(N)e^{i(\alpha p^2 + \beta p)}e^{-i[\alpha(p-v)^2 + \beta(p-v)]}EV^\dagger(N) \\ &= V(N)e^{i(2\alpha vp + \beta v - \alpha v^2)}EV^\dagger(N) \\ &= e^{i(\beta v - \alpha v^2)}V(x/a)e^{i2\alpha vp}EV^\dagger(x/a) \\ &= e^{i(\beta v - \alpha v^2)}V(x/a)e^{i2\alpha vp}EV^\dagger(x/a) \\ &= e^{i\beta v - \alpha v^2}V(x/a)V^\dagger\left(\frac{x+2\alpha v}{a}\right)e^{iqap}E. \end{aligned} \quad (\text{A8})$$

This is a closed result within the space of lattice translations if $2\alpha v = qa$, $q \in \mathcal{Z}$. The transformed E is:

$$\begin{aligned} UEU^\dagger &= e^{i\beta v - \alpha v^2}V(N)V^\dagger(N+q)T^qE \\ &= e^{i\beta v - \alpha v^2}V(N)V^\dagger(N+q)ET^qe^{ivaq} \\ &= e^{i(\beta v - \alpha v^2 + vaq)}V(N)V(N+q)ET^q \\ &= e^{i(\beta v - qav/2 + vaq)}V(N)V^\dagger(N+q)ET^q \\ &= e^{i\chi q}V(N)V(N+q)ET^q. \end{aligned} \quad (\text{A9})$$

Therefore, the new Hamiltonian becomes:

$$\tilde{H} = V(N)V^\dagger(N+1)T + \Lambda e^{i\chi_q}V(N)V^\dagger(N+q)ET^q + h.c. \quad (\text{A10})$$

which is a multiple neighbor tight-binding operator. Since the parameters in U can be chosen at will, we have that for $q = 1$ or $q = -1$, H reduces to a nearest-neighbor Hamiltonian. Finally, we recognize that every nearest-neighbor tight-binding model in 1D can be cast in the form of a Hamiltonian with real and positive couplings by means of gauge transformation. In general, we have

$$\Delta = V(N)V^\dagger(N+1) (1 + \Lambda e^{\pm i\chi_q} e^{\pm i\omega N}). \quad (\text{A11})$$

We recognize the unitary nature of $V(N)$ so $VV^\dagger = \mathbf{1}$ implies $V = \exp(i\Phi(N))$ and $V(N)V^\dagger(N+1) = \exp\{i(\Phi(N) - \Phi(N+1))\} \equiv \exp(-i\delta\Phi(N))$ which is only a phase factor, and then

$$\Delta = e^{i\Omega(N)} |\Delta(N)|, \quad \tilde{U} = e^{i\sum_{j=-\infty}^n \Omega(N+j)} \quad (\text{A12})$$

$$T\tilde{U}^\dagger = e^{-i\sum_{j=\infty}^{n+1} \Omega(N+j)} iT \quad (\text{A13})$$

$$\tilde{U}T\tilde{U}^\dagger = e^{-i\Omega(N+n+1)} T. \quad (\text{A14})$$

If we choose $n = -1$ we obtain the following expression for $|\Delta|$

$$|\Delta| = \sqrt{1 + \Lambda^2 + 2\Lambda \cos(\omega N + \chi_\pm)}, \quad (\text{A15})$$

which is the sought expression. Geometric deformations are therefore equivalent to on-site quasiperiodic energies.

In the case of a very faint intensity of the potential, we can analyze the limit $\Lambda \ll 1$ and provide an expression

for the coupling:

$$|\Delta| \simeq 1 + \Lambda \cos(\omega N + \chi_\pm), \quad \Lambda \ll 1, \quad (\text{A16})$$

which is in full agreement with the first corrections to the effective coupling in the problem of rotating dimers.

Appendix B: Box-counting fractal dimension calculation

The fractal dimensions of the symmetric and antisymmetric spectra of the chain made of dimers were calculated using the method of box counting:

$$N(s) = \left(\frac{1}{s}\right)^D, \quad (\text{B1})$$

where N is the number of boxes and s is the size of one box. Thus the fractal dimension can be calculated as follows:

$$D = \frac{\log N(s)}{\log(1/s)}. \quad (\text{B2})$$

The fractal dimensions for specific values of $\omega(N-1)/2\pi$ of the spectrum showed Fig. 1 (b) are presented in Fig. 14. The range of values of the fractal dimensions for the symmetric mode band are reported in Table I.

-
- [1] L. Tagliacozzo, A. Celi, P. Orland, M. W. Mitchell, and M. Lewenstein, *Nature Communications* **4**, 2615 (2013).
- [2] W. Greiner and S. S. E. Stein, *Quantum Chromodynamics* (Springer, 2007).
- [3] D. Epple, C. Feuchter, and H. Reinhardt, *AIP Conf. Proc.* **756**, 269 (2005).
- [4] T. Kugo and I. Ojima, *Prog. Theor. Phys. Suppl.* **66**, 1 (1979).
- [5] M. Frasca, (2014), arXiv:1409.2351 [math-ph].
- [6] M. Frasca, *Mod. Phys. Lett. A* **24**, 2425 (2009).
- [7] M. A. Kasevich, E. Riis, S. Chu, and R. G. DeVoe, *Phys. Rev. Lett.* **63**, 612 (1989).
- [8] A. Clairon, C. Salomon, S. Guellati, and W. D. Phillips, *EPL* **16**, 165 (1991).
- [9] P. Bienstman, S. Assefa, S. G. Johnson, J. D. Joannopoulos, G. S. Petrich, and L. A. Kolodziejski, *J. Opt. Soc. Am. B* **20**, 1817 (2003).
- [10] K. Jiménez-García, L. J. LeBlanc, R. A. Williams, M. C. Beeler, A. R. Perry, and I. B. Spielman, *Phys. Rev. Lett.* **108**, 225303 (2012).
- [11] A. Perez-Leija, R. Keil, A. Kay, H. Moya-Cessa, S. Nolte, L.-C. Kwek, B. M. Rodríguez-Lara, A. Szameit, and D. N. Christodoulides, *Phys. Rev. A* **87**, 012309 (2013).
- [12] F. Dreisow, M. Heinrich, R. Keil, A. Tünnermann, S. Nolte, S. Longhi, and A. Szameit, *Phys. Rev. Lett.* **105**, 143902 (2010).
- [13] Y. Hernández-Espinosa, A. S. Rosado, and E. Sadurní, *J. Phys. A: Math. Theor.* **49**, 485201 (2016).
- [14] K. K. Gomes, W. Mar, W. Ko, F. Guinea, and H. C. Manoharan, *Nature* **483**, 306 (2012).
- [15] J. Struck, C. Ölschläger, M. Weinberg, P. Hauke, J. Simonet, A. Eckardt, M. Lewenstein, K. Sengstock, and P. Windpassinger, *Phys. Rev. Lett.* **108**, 225304 (2012).
- [16] L. Fallani, J. E. Lye, V. Guarrera, C. Fort, and M. Inguscio, *Phys. Rev. Lett.* **98**, 130404 (2007).
- [17] M. Bellec, U. Kuhl, G. Montambaux, and F. Mortessagne, *Phys. Rev. B* **88**, 115437 (2013).
- [18] S. Bittner, B. Dietz, M. Miski-Oglu, P. Oria Iriarte, A. Richter, and F. Schäfer, *Phys. Rev. B* **82**, 014301 (2010).
- [19] J. A. Franco-Villafañe, E. Sadurní, S. Barkhofen, U. Kuhl, F. Mortessagne, and T. H. Seligman, *Phys. Rev. Lett.* **111**, 170405 (2013).
- [20] M. I. Katsnelson, K. S. Novoselov, and A. K. Geim, *Nature Physics* **2**, 620 (2006).
- [21] A. K. Geim and K. S. Novoselov, *Nature Materials* **6**, 183 (2007).
- [22] A. H. Castro Neto, F. Guinea, N. M. R. Peres, K. S. Novoselov, and A. K. Geim, *Rev. Mod. Phys.* **81**, 109

- (2009).
- [23] M. I. Katsnelson, *Mater. Today* **10**, 20 (2007).
- [24] M. I. Katsnelson, *Eur. Phys. J. B* **51**, 157 (2006).
- [25] R. Peierls, *Z. Phys.* **80**, 763 (1933).
- [26] P. G. Harper, *Proc. Phys. Soc. A* **68**, 874 (1955).
- [27] Y. Last, *Proc. XIth Int. Congress of Mathematical Physics (Paris 1994)*, 366 (1995).
- [28] M. Y. Azbel, *JETP* **19**, 634 (1964).
- [29] D. R. Hofstadter, *Phys. Rev. B* **14**, 2239 (1976).
- [30] O. Richoux and V. Pagneux, *Europhys. Lett.* **59**, 34 (2002).
- [31] X. Ni, K. Chen, M. Weiner, D. J. Apigo, C. Prodan, A. Alù, E. Prodan, and A. B. Khanikaev, *Commun. Phys.* **2**, 55 (2019).
- [32] U. Kuhl and H.-J. Stöckmann, *Phys. Rev. Lett.* **80**, 3232 (1998).
- [33] A. Avila and S. Jitomirskaya, in *Mathematical Physics of Quantum Mechanics*, edited by J. Asch and A. Joye (Springer Berlin Heidelberg, 2006) pp. 5–16.
- [34] S. Deng, A. Simon, and J. Köhler, *J Solid State Chem.* **176**, 412 (2003).
- [35] E. Rivera-Mociños and E. Sadurní, *J. Phys. A* **49**, 175302 (2016).
- [36] E. Sadurní, T. H. Seligman, and F. Mortessagne, *New Journal of Physics* **12**, 053014 (2010).
- [37] U. Kuhl, S. Barkhofen, T. Tudorovskiy, H.-J. Stöckmann, T. Hossain, L. de Forges de Parny, and F. Mortessagne, *Phys. Rev. B* **82**, 094308 (2010).
- [38] S. Barkhofen, M. Bellec, U. Kuhl, and F. Mortessagne, *Phys. Rev. B* **87**, 035101 (2013).
- [39] M. Bellec, U. Kuhl, G. Montambaux, and F. Mortessagne, *Phys. Rev. B* **88**, 115437 (2013).
- [40] A. P. Sutton, *Electronic Structure of Materials* (Oxford University Press, 1993).
- [41] A. Avila and K. Raphaël, *Annals of Mathematics* **164**, 911 (2006).
- [42] E. Sadurní and Y. Hernández-Espinosa, *J. Phys. A: Math. Theor.* **52**, 295204 (2019).
- [43] Y. Hernández-Espinosa, R. A. Méndez-Sánchez, and E. Sadurní, *J. Phys. B: At. Mol. Opt. Phys.* **53**, 105101 (2020).
- [44] R. Rajaraman, *Solitons and instantons. An introduction to Solitons and Instantons in Quantum Field Theory* (North-Holland, 1987).
- [45] A. C. Scott, F. Y. F. Chu, and D. W. McLaughlin, *Proc. IEEE* **61**, 1443 (1973).
- [46] F. Ramírez-Ramírez, E. Flores-Olmedo, G. Báez, E. Sadurní, and R. A. Méndez-Sánchez, *Sci. Rep.* **10**, 10229 (2020).
- [47] V. A. Miransky and I. A. Shovkovy, *Phys. Rep.* **576**, 1 (2015).
- [48] D. J. Thouless, M. Kohmoto, M. P. Nightingale, and M. den Nijs, *Phys. Rev. Lett.* **49**, 405 (1982).